International Journal of Computational and Experimental Science and ENgineering (IJCESEN)

Vol. 12-No.2 (2026) pp. 709-716
http://www.ijcesen.com

ISSN: 2149-9144

Research Article

Integrated Seismic Refraction and Electrical Resistivity Survey for Geotechnical Zonation of a Large Industrial Site in Western Algeria

Leila Benhenni*, Saddek Samai[2], Leila Bouchama[3]

[1] University of Sciences and Technology Houari Boumediene, Geophysics Department, 16000, Algiers-Algeria
* **Corresponding Author Email:** lbenhenni@usthb.dz - **ORCID:** orcid.org/0009-0001-3691-159X

[2] University of Sciences and Technology Houari Boumediene, Geophysics Department, 16000, Algiers-Algeria
Email: ssamai@usthb.dz - **ORCID:** orcid.org/0009-0004-7532-8008

[3] University of Sciences and Technology Houari Boumediene, Laboratory of Cities, Regions and Territorial Governance (LVRGT), 16000, Algiers-Algeria
Email: lbouchama@usthb.dz - **ORCID:** orcid.org/0009-0009-9668-645X

Article Info:

DOI: 10.22399/ijcesen.5273
Received : 20 March 2026
Received : 28 May 2026
Accepted : 03 June 2026

Keywords

seismic refraction
vertical electrical sounding
dynamic elastic parameters
geotechnical zonati
western Algeria

Abstract:

Integrated geophysical surveys were conducted over a 300-hectare industrial development site in western Algeria to characterize subsurface conditions in heterogeneous Miocene formations. Eleven vertical electrical soundings (Wenner configuration; maximum electrode spacing AB = 300 m) and three representative seismic refraction profiles were acquired, providing complementary velocity and resistivity constraints down to 50 m depth.A consistent three-layer subsurface model was identified across the site: a surface silty sand horizon (Vp = 300–2000 m/s; ρ = 80–2000 Ω·m; 3–4 m thick), an intermediate sandstone and calcareous tuff layer (Vp = 1000–2000 m/s; ρ = 100–900 Ω·m; 8–25 m thick), and a consolidated Miocene sandstone substratum (Vp = 1100–4560 m/s; ρ = 15–130 Ω·m). The substratum top varies from +31.8 m to +59.5 m elevation.Dynamic elastic parameters derived from empirical Vp–Vs relationships indicate significant lateral variability in mechanical competence (Young's modulus E = 0.5–22 GPa; Poisson's ratio ν = 0.27–0.48). A statistically significant resistivity–velocity correlation (R^2 = 0.76) confirms dataset consistency. Four engineering zones (A–D) are delineated, ranging from very competent sandstone suitable for heavy direct foundations (Zone A) to water-saturated altered materials requiring drainage and ground improvement (Zone D). These results provide a quantitative geotechnical framework for rational foundation design across the site.

1.Introduction

Industrial infrastructure development in the western Mediterranean coastal zone of Algeria requires rigorous subsurface characterization to ensure foundation safety and structural performance [11]. The Miocene formations dominating this region alternating sandstones, calcareous tuffs, marls, and bioclastic limestones exhibit pronounced lithological heterogeneity compounded by diagenetic alteration, variable water saturation, and irregular paleotopography. These conditions render single-method or borehole-only investigations insufficient for site-scale geotechnical assessment.Seismic refraction and vertical electrical sounding (VES) are established non-invasive tools for subsurface characterization in shallow engineering geology [19],[21]. Seismic refraction yields compressional P-wave velocities (Vp) directly related to formation stiffness, while VES characterizes the vertical resistivity distribution and enables discrimination of lithology, water content, and clay fraction. Their joint interpretation resolves ambiguities inherent in each method applied independently [15],[7].Integrated geophysical approaches have been successfully applied to site investigations across North Africa. Boubaya et al. (2017) [3] showed that joint seismic–resistivity interpretation significantly improved basement delineation in sandstone terrains of northern Algeria. Fehdi et al. (2011) [8] reported a strong velocity–resistivity correlation in Miocene formations of eastern Algeria, validating empirical elastic parameter estimation. Gabtni et al. (2021) [9] used integrated profiles for port infrastructure characterization in Tunisia, and Khadrouf et al. (2024) [4] applied a comparable workflow to industrial site zonation in Morocco. Khalil et al (2016) [12] established a methodological framework for dynamic parameter derivation in semi-consolidated sedimentary sequences that has been widely adopted in North African applied geophysics.

Despite this body of work, integrated studies specifically combining seismic refraction and electrical resistivity for large industrial developments in western Algeria remain scarce. The present study addresses this gap through multi-method geophysical investigation of a 300-hectare site, with three principal contributions: (i) joint acquisition and integrated interpretation of seismic refraction and electrical datasets over a site with significant lateral geological variability; (ii) systematic derivation and spatial mapping of dynamic elastic parameters; and (iii) a quantitative geotechnical zoning map linking geophysical measurements to foundation design requirements.Beyond its regional significance, this study demonstrates the applicability of integrated seismic–electrical approaches for rapid pre-construction geotechnical assessment in heterogeneous coastal sedimentary environments, particularly in regions where borehole coverage remains limited.

2. Geological Context

The study site is located in western Algeria within a Mediterranean coastal domain. Regional geology is dominated by Miocene formations of alternating sandstones, sands, marls, and bioclastic limestones, overlain by Quaternary alluvial sandy and silty deposits. These sequences were deposited in shallow marine to paralic environments during the Serravallian–Tortonian stages and subsequently affected by diagenetic cementation of variable intensity, producing the marked lateral heterogeneity observed in this study. The interpreted lithological sequence is consistent with regional Miocene stratigraphy described in nearby outcrops and previous geological mapping studies of the western Algerian margin .Site topography is sub-horizontal, with station elevations between 62 and 93 m above sea level. The proximity to the Mediterranean coast introduces marine moisture into shallow formations, which may locally influence the electrical properties of near-surface materials. The morphologically flat terrain facilitated systematic acquisition of all planned profiles and soundings. The location map is presented in Fig. 1.

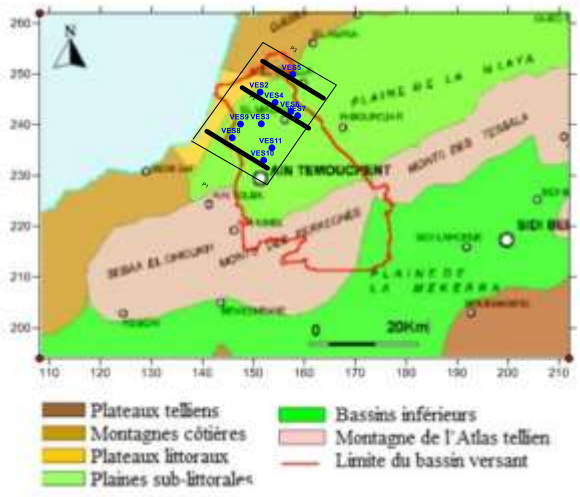

Figure 1. *Location map of seismic refraction profiles (P3, P6, P11) and vertical electrical soundings (VES1–VES11). UTM coordinates, Western Algeria.*

3. Materials and Methods

3.1 Seismic Refraction

Eleven seismic refraction profiles were acquired across the site; three representative profiles (P3, P6, P11) are presented here to illustrate the full range of lithological and geotechnical conditions. Each profile comprised several seismic bases of 12 traces, with 14 Hz vertical geophones at 5 m inter-geophone spacing (55 m total spread length), connected to a 24-channel engineering seismograph with a sampling interval of 0.25 ms. A sledgehammer source (5 kg) on a steel base plate was used, with a minimum of five stacks per shot point to improve the signal-to-noise ratio. Forward and reverse shots were fired at each end of every base, enabling reciprocal traveltime verification.First-arrival P-wave traveltimes were manually picked on field seismograms. Layer velocities and thicknesses were determined by graphical time–distance (T–X) analysis using the delay-time method for dipping refractors [21],[18].

3.1.1 Estimation of Shear-Wave Velocity and Dynamic Elastic Parameters

Since direct S-wave measurements were not performed, shear-wave velocities (Vs) were estimated from Vp using the empirical mudrock-line relationship of Castagna et al. (1985) [6], calibrated for clastic silicate rocks:

$$Vs = 0.804 \times Vp - 855.9 \quad (m/s) \qquad (1)$$

Formation densities were estimated using the relationship of Gardner et al. (1974) [11]:

$$\rho = 0.31 \times Vp^{0.25} \quad (g/cm^3) \qquad (2)$$

(ρ in g/cm³, Vp in m/s)

It must be noted that the Castagna et al. (1985) [6] relationship was originally calibrated for brine-saturated sandstones and may introduce systematic errors when applied to partially saturated or tuffaceous materials (Zones C and D). The dynamic elastic parameters derived here should therefore be considered approximate dynamic estimates, pending direct Vs measurement by MASW or cross-hole methods. Uncertainty ranges are reported in Table 3.

Dynamic elastic parameters were computed using the standard isotropic elastic relations:

$$\nu = [(Vp/Vs)^2 - 2] / \{2[(Vp/Vs)^2 - 1]\} \qquad (3)$$

$$E = 2\rho Vs^2(1 + \nu) \qquad (4)$$

3.2 Vertical Electrical Soundings

Eleven soundings (VES1–VES11) were performed using the Wenner configuration with maximum current electrode half-spacing AB/2 = 150 m, yielding investigation depths of 40–50 m. Apparent resistivity was calculated as $\rho a = 2\pi a \times (\Delta V/I)$, where a is the electrode spacing. Field curves were interpreted by 1D least-squares inversion assuming horizontal stratification; the RMS inversion error ranged between 3% and 8%, indicating satisfactory agreement between observed and calculated apparent resistivities. Three lateral resistivity maps were constructed at AB = 30 m, AB = 90 m, and AB = 300 m.

3.3 Data Processing

All processing, interpolation, and figure generation used Python 3.11, with NumPy [14], Matplotlib [16], SciPy [22], and PyGIMLi [20]. The resistivity–velocity correlation (Fig. 8) was generated by pairing co-located VES apparent resistivity at AB = 90 m with average Layer 2 Vp from the nearest profile, yielding 11 independent data pairs.

4. Results

4.1 Integrated Geoseismic and Geoelectrical Sections

Figs. 2–4 present the integrated sections for the three representative profiles, each showing the interpreted seismic refraction model superimposed with the corresponding vertical electrical sounding data. This joint representation highlights the complementarity of velocity and resistivity constraints and facilitates direct lithological correlation between the two datasets. Three seismic layers are consistently identified across all profiles (Table 1):

- Layer 1: Silty sand (Vp = 300–2000 m/s; thickness 2–4 m): Loose Quaternary alluvial deposits with high porosity and low seismic velocity. Correspondingly high resistivities (80–900 Ω·m) reflect unsaturated near-surface conditions.
- Layer 2: Sandstone / calcareous tuff (Vp = 1000–1960 m/s; thickness 8–25 m): The principal load-bearing unit. Lateral velocity variation reflects the northeast-to-central transition from cemented sandstone to calcareous tuff. Resistivities of 100–900 Ω·m are consistent with variable cementation and partial saturation.
- Layer 3: Consolidated Miocene sandstone substratum (Vp = 1100–4560 m/s): The deepest refractor. Lower velocities in the west (~1400 m/s) reflect weathering or partial saturation; high velocities in the northeast (~4500 m/s) indicate very compact dry sandstone. Resistivities range from 15–130 Ω·m, with the lowest values in the west reflecting higher water saturation or clay content.

***Table 1**. Summary of P-wave velocities and layer thicknesses for the three representative seismic profiles.*

Profile	Orient.	Layer 1 Lith.	Vp1 (m/s)	Layer 2 Lith.	Vp2 (m/s)	Layer 3 Lith.	Vp3 (m/s)	Thick. L1/L2 (m)
P3	NW–SE	Silty sand	800–1120	Cemented sandstone	1560–1900	Compact sandstone substratum	3500–4400	3 / 10 / 18
P6	NW–SE	Silty sand	400–700	Calcareous tuff	1300–1600	Consolidated sandstone substratum	2200–2800	3 / 12 / 15
P11	NW–SE	Silty sand	700–800	Altered sandstone	1000–1500	Weathered sandstone substratum	2900–3300	3 / 15 / —

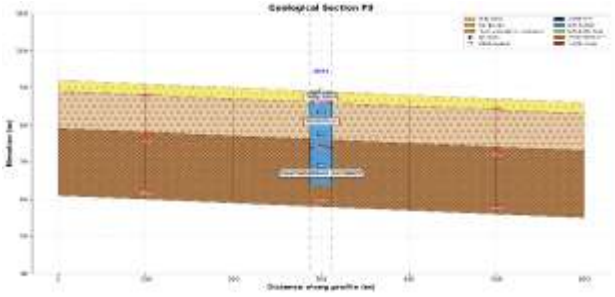

***Figure 2**. Integrated geoseismic and geoelectrical section, profile P3 (northeast). Upper panel: seismic refraction model — silty sand (800–1120 m/s) / cemented sandstone (1560–1900 m/s) / compact sandstone substratum (3500–4400 m/s). Lower panel: superimposed VES3 geoelectrical column — high resistivities (ρ2 = 400 Ω·m, ρ3 = 2000 Ω·m) confirm compact dry sandstone, consistent with the highest Vp values on site (Zone A).*

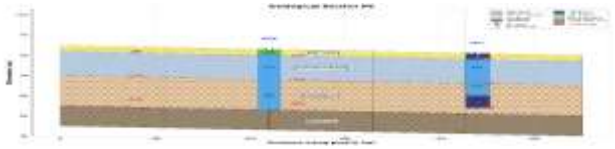

***Figure 3**. Integrated geoseismic and geoelectrical section, profile P6 (central). Upper panel: seismic refraction model — silty sand (400–700 m/s) / calcareous tuff (1300–1600 m/s) / consolidated sandstone substratum (2200–2800 m/s). Lower panel: superimposed VES6 and VES7 geoelectrical columns — intermediate resistivities (200–900 Ω·m) consistent with calcareous tuff and sandstone interbeds (Zone C).*

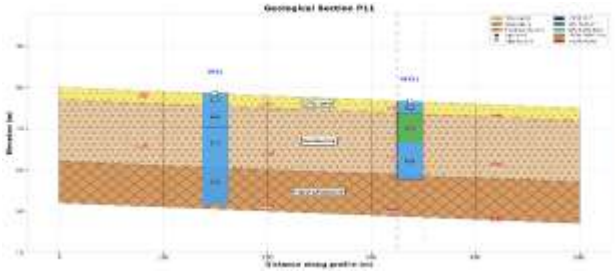

***Figure 4**. Integrated geoseismic and geoelectrical section, profile P11 (west). Upper panel: seismic refraction model — silty sand (700–800 m/s) / altered sandstone (1000–1500 m/s) / weathered sandstone substratum (2900–3300 m/s). Lower panel: superimposed VES11 and VES1 geoelectrical columns — moderate resistivities (100–700 Ω·m) indicate altered, partially saturated sandstone (Zone D).*

4.2 Substratum Velocity Map

Fig. 5 shows the interpolated 3D velocity map of the consolidated Miocene sandstone substratum, based on third-layer Vp from all eleven profiles. Velocities increase from ~1400 m/s (west, weathered) to >4500 m/s (northeast, compact and dry), directly reflecting the degree of diagenetic cementation.

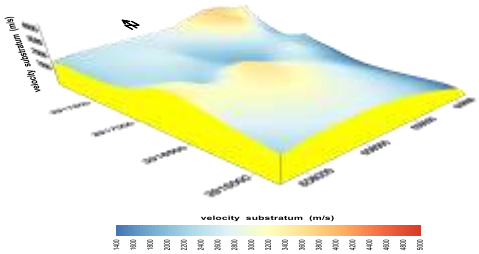

***Figure 5.** 3D velocity map of the consolidated Miocene sandstone substratum (m/s). Red: maximum velocities, northeast sector (compact dry sandstone). Blue: minimum velocities, western sector (weathered/saturated sandstone).*

4.3 Vertical Electrical Sounding Results

The 1D geoelectrical columns for the five key soundings are presented in the integrated sections of Figs. 2–4 (superimposed on the corresponding seismic profiles). The three-layer electrical stratigraphy is spatially consistent with the seismic model across all profiles. Table 2 summarizes layer resistivities, interpreted basement depth, and computed top elevation.

4.4 Substratum Top Map

Fig. 6 presents the isohypse map of the consolidated Miocene sandstone substratum top, interpolated from all VES depth solutions. The top elevation varies from +31.8 m (VES5, south-central) to +59.5 m (VES11, west), with a well-defined N–S elongated paleotopographic depression in the central sector.

***Table 2**. Resistivities (Ω·m) per layer, interpreted basement depth, and top elevation for key soundings. Inversion RMS error: 3–8%.*

Sounding	Profile	Z (m)	ρ1	ρ2	ρ3	ρ4	ρ5	Depth (m)	Elev. (m)	Lithological Interpretation
VES3	P3	82.2	80	400	200	130	40	28	54.2	Silty sand / Sandstone / Clay
VES6	P6	68.1	900	200	–	–	110	30	38.1	Silty sand / Tuff / Clay / Sandstone
VES7	P6	66.5	80	300	130	70	80	27	39.5	Silty sand / Tuff / Sandstone / Clay
VES11	P11	79.5	260	500	170	160	–	20	59.5	Silty sand / Sandstone
VES1	P11	80.0	290	170	400	170	40	27	53.0	Silty sand / Sandstone / Clay

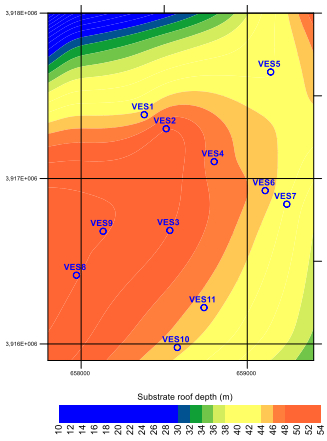

***Figure 6**. Isohypse map of the consolidated Miocene sandstone substratum top elevation (m, contour interval 2 m). VES1–VES11 locations shown with interpreted top elevations. A central N–S depression is clearly delineated.*

4.5 Resistivity Maps

Fig. 7 presents lateral resistivity maps at three investigation depths, revealing the spatial extent of compact resistive sandstone in the northeast quadrant and the progressive deepening of conductive clay-rich horizons.

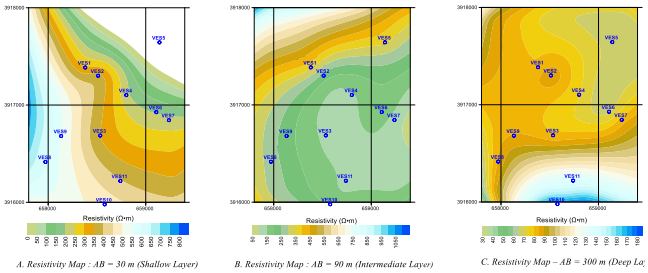

***Figure 7.** Lateral resistivity maps at: (a) AB = 30 m (0–5 m depth); (b) AB = 90 m (10–15 m); (c) AB = 300 m (40–50 m). Scale in Ω·m. Northeast quadrant shows consistently high resistivities at all depths.*

4.6 Resistivity–Velocity Correlation

Fig. 8 presents the scatter plot of apparent resistivity (AB = 90 m) against Layer 2 Vp for the eleven co-located pairs. The positive correlation ($R^2 = 0.76$, $p < 0.01$) is consistent with compaction-driven reduction in porosity, which simultaneously increases elastic stiffness and decreases pore-fluid connectivity, thereby raising both Vp and resistivity. The residual scatter reflects the additional influence of clay content and mineralogy, which reduce resistivity through surface conductance independently of porosity effects.

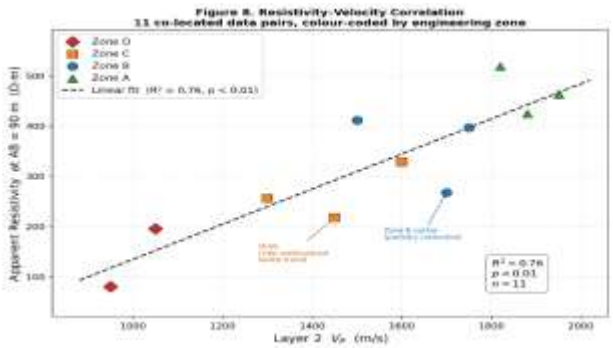

***Figure 8**. Scatter plot: apparent resistivity (AB = 90 m, Ω·m) vs. Layer 2 Vp (m/s) for 11 co-located pairs. Linear fit: $R^2 = 0.76$, $p < 0.01$. Points colour-coded by engineering zone (A–D).*

4.7 Dynamic Elastic Parameters and Engineering Zonation

Table 3 summarizes estimated dynamic elastic parameters by zone. Uncertainty ranges (±) for Young's modulus reflect propagated velocity measurement uncertainty (±50 m/s). The notation † indicates Poisson's ratio values approaching the theoretical incompressibility limit (~0.5), physically consistent with partial to full water saturation in Zone D; these values are approximate owing to the use of empirically estimated Vs.

***Table 3**. Dynamic elastic parameters by engineering zone. High ν values in Zone D reflect partial saturation and weakly consolidated materials; values are approximate.*

Zone	Profiles	Vp (m/s)	Vs est. (m/s)	ρ (g/cm³)	ν	E (GPa)	Lithology	Foundation Recommendation
A	P3	3500–4400	1958–2390	2.38–2.45	0.27–0.30	14–22 ±3	Compact dry sandstone	Heavy direct foundations
B	P1, P2	2000–3500	750–1960	2.10–2.38	0.30–0.40	3–14 ±2	Moderately compact sandstone	Standard shallow foundations
C	P6	1300–1960	190–720	2.0–2.1	0.40–0.45	0.5–3 ±1	Calcareous tuff / Sandstone	Adapted design; raft or piles
D	P11	800–1500	—	1.85–1.95	0.45–0.48†	<0.5 ±0.2	Silty sand / Weathered sandstone	Drainage + ground reinforcement

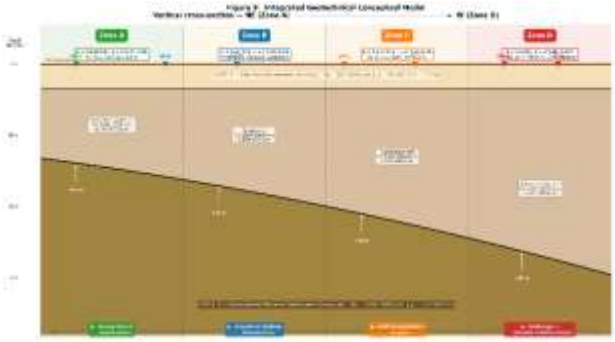

***Figure 9**. Integrated geotechnical conceptual model of the site. Vertical cross-section showing the three-layer stratigraphy with Vp and resistivity ranges, substratum elevation, and engineering zone boundaries (A–D) with foundation recommendations.*

5. Discussion

5.1 Geological Interpretation

The three-layer model is consistent with regional Miocene stratigraphy of western Algeria. Layer 1 corresponds to Quaternary reworking of Miocene sandy substrate, common throughout the North African Mediterranean coastal plain [3]. Layer 2 exhibits a northeast-to-central facies transition from compact cemented sandstone to calcareous tuff, consistent with the heterogeneous shallow marine depositional environment of Serravallian–Tortonian sequences. The consolidated sandstone substratum reaches Vp values up to 4560 m/s in the northeast — comparable to values for compact Miocene sandstones reported by Fehdi et al. (2020) [8] and Gabtni et al. (2013) [9], while lower values in the west reflect weathering and partial saturation, not an absence of the competent lithology.

5.2 Velocity–Resistivity Correlation

The $R^2 = 0.76$ correlation confirms that porosity is the dominant control on both elastic stiffness and electrical conductivity across the site, consistent with Archie's Law [1] and effective medium theory [18]. The scatter around the regression line reflects the secondary influence of clay content, which reduces resistivity through surface conductance independently of porosity a well-documented phenomenon in argillaceous sandstones [12],[4]. These R^2 values are consistent with the range of 0.65–0.82 reported for comparable Miocene sandstone settings in North Africa.

5.3 Dynamic Elastic Parameters

Young's modulus spans nearly two orders of magnitude (E = 0.5–22 GPa), quantifying the extreme mechanical contrast between loose surface sands and compact northeast sandstone. Zone A values (E = 14–22 GPa) compare favourably with compact Miocene sandstone data reported by Brocher (2005) [6] and Fehdi et al. (2020) [9], confirming suitability for heavy direct foundations. Zone C (E = 0.5–3 GPa) corresponds to calcareous tuff values documented across Mediterranean Miocene settings [10], where raft or pile foundations are standard practice. In Zone D, Poisson's ratio approaching 0.48 is physically consistent with a water-saturated granular medium [2], corroborated by low resistivities (100–700 Ω·m) at VES11 and VES1.

5.4 Geotechnical Implications

The four-zone classification directly informs construction planning:

- Zone A: Excellent competence. Heavy industrial loads storage tanks, manufacturing halls, process equipment can be founded directly on shallow spread footings.
- Zone B: Good competence. Standard shallow foundations with bearing capacity verification by in situ testing (SPT or PMT) are recommended.

- Zone C: Moderate competence with calcareous tuff. Raft foundations or cement grouting are advised to mitigate differential settlement risk under infiltration.
- Zone D: Poor competence, high saturation. Dewatering, dynamic compaction or vibroflotation, and a permanent drainage network are required before any structural foundation.

5.5 Engineering Significance of the Structural Depression

The central N–S paleotopographic depression in the substratum map (Fig. 6) represents a zone of elevated differential settlement risk, where the substratum top varies by more than 15 m over lateral distances of less than 50 m. Foundation design across the central sector must account for this abrupt variation, particularly for continuous structural elements such as industrial pavements and pipeline networks.

5.6 Limitations

- Absence of direct Vs measurements: The Castagna et al. (1985) [7] empirical relationship may not accurately represent calcareous tuff (Zone C) or saturated altered sandstone (Zone D). MASW surveys are strongly recommended before detailed design.
- No borehole control: Lithological interpretations are based on geophysical response and regional geological analogy. Cored boreholes with laboratory testing are recommended in Zones C and D.
- 1D VES assumption: Horizontal stratification assumed in inversion may introduce depth errors where significant lateral gradients exist. 2D ERT profiles would improve resolution of lateral discontinuities.
- Spatial interpolation: Accuracy of interpolated maps between measurement locations cannot be independently verified without additional data.

6. Conclusions

An integrated seismic refraction and electrical resistivity survey has characterized the subsurface geotechnical conditions of a 300-hectare industrial development site in western Algeria. The principal conclusions are:

1. A consistent three-layer model surface silty sand (3–4 m), intermediate sandstone–tuff (8–25 m), and consolidated Miocene sandstone substratum is identified across the entire site.
2. The substratum top varies from +31.8 m to +59.5 m elevation, with a central N–S paleotopographic depression representing an elevated differential settlement risk zone.
3. A statistically significant resistivity–velocity correlation (R^2 = 0.76) confirms the consistency of the joint dataset and validates the integrated geological interpretation.
4. Estimated dynamic elastic parameters (E = 0.5–22 GPa; ν = 0.27–0.48) support the delineation of four engineering zones (A–D) with contrasting geotechnical suitability and specific foundation recommendations.
5. The integration of seismic refraction and electrical resistivity proved effective for resolving both lithological variability and geotechnical heterogeneity in complex Miocene terrains, demonstrating the value of multi-method geophysics for sustainable industrial land-use planning.

Complementary investigations — MASW for direct Vs measurement, 2D ERT profiling, geotechnical boreholes, and in situ pressuremeter testing — are strongly recommended in Zones C and D before detailed foundation design.

Author Statements

- **Ethical approval:** The conducted research is not related to either human or animal use.
- **Conflict of interest:** The authors declare that they have no known competing financial interests or personal relationships that could have appeared to influence the work reported in this paper.
- **Acknowledgement:** The authors declare that they have nobody or no-company to acknowledge.
- **Author contributions:** Conceptualization, field acquisition, data processing, interpretation, and manuscript preparation were carried out by the author(s). All authors have read and agreed to the published version of the manuscript.
- **Funding information:** The authors declare that there is no funding to be acknowledged.
- **Data availability statement:** The data that support the findings of this study are available on request from the corresponding author. The data are not publicly available due to privacy or ethical restrictions.

References

[1] Archie, G. E. (1942). The electrical resistivity log as an aid in determining some reservoir characteristics. Transactions of the AIME, 146(1), 54–62. DOI:10.2118/942054-G

[2] Biot, M. A. (1956). Theory of propagation of elastic waves in a fluid-saturated porous solid. Journal of the Acoustical Society of America, 28(2), 168–178. DOI:10.1121/1.1908239

[3] Boubaya, D. (2017). Combining Resistivity and Aeromagnetic Geophysical Surveys for Groundwater Exploration in the Maghnia Plain of Algeria. *Journal of Geological Research*, 2017, Article ID 1309053. DOI: 10.1155/2017/1309053

[4] Khadrouf, I., El Hammoumi, O., El Goumi, N., et al. (2024). Enhancing geotechnical zoning through near-surface geophysical surveys: a case study from eastern Agadir, Morocco. *Mediterranean Geoscience Reviews*, 6, 279–300. DOI: 10.1007/s42990-024-00137-3

[5] Brocher, T. M. (2005). Empirical relations between elastic wavespeeds and density in the Earth's crust. Bulletin of the Seismological Society of America, 95(6), 2081–2092. DOI:10.1785/0120050077

[6] Castagna, J. P., Batzle, M. L., & Eastwood, R. L. (1985). Relationships between compressional-wave and shear-wave velocities in clastic silicate rocks. Geophysics, 50(4), 571–581. DOI:10.1190/1.1441933

[7] Loke, M. H., Chambers, J. E., Rucker, D. F., Kuras, O., & Wilkinson, P. B. (2013). Recent developments in the direct-current geoelectrical imaging method. *Journal of Applied Geophysics*, 95, 135–156. DOI: 10.1016/j.jappgeo.2013.02.017

[8] Fehdi, C., Baali, F., Boubaya, D., & Rouabhia, A. (2011). Detection of sinkholes using 2D electrical resistivity imaging in the Cheria Basin (north-east of Algeria). *Arabian Journal of Geosciences*, 4(1–2), 181–187. DOI: 10.1007/s12517-009-0117-2

[9] Gabtni, H., Jallouli, C., Mickus, K. L., Zouari, H., & Turki, M. M. (2013). Geodynamics of the Southern Tethyan Margin in Tunisia and Maghrebian domain: new constraints from integrated geophysical study. *Arabian Journal of Geosciences*, 6, 271–286. DOI: 10.1007/s12517-011-0362-

[10] Gardner, G. H. F., Gardner, L. W., & Gregory, A. R. (1974). Formation velocity and density — the diagnostic basics for stratigraphic traps. Geophysics, 39(6), 770–780. DOI:10.1190/1.1440465

[11] Hadji, R., Boumazbeur, A., Limani, Y., Baghem, M., Chouabi, A., & Demdoum, A. (2013). Geologic, topographic and climatic controls in landslide hazard assessment using GIS modelling: a case study of Souk Ahras region, NE Algeria. *Quaternary International*, 302, 224–237. DOI: 10.1016/j.quaint.2012.11.027

[12] Khalil, M. H., & Hanafy, S. M. (2016). Geotechnical Parameters from Seismic Measurements: Two Field Examples from Egypt and Saudi Arabia. *Journal of Environmental and Engineering Geophysics*, 21(1), 13–28. DOI: 10.2113/JEEG21.1.13

[13] Harris, C. R., Millman, K. J., van der Walt, S. J., et al. (2020). Array programming with NumPy. Nature, 585, 357–362. DOI:10.1038/s41586-020-2649-2

[14] Hunter, J. D. (2007). Matplotlib: A 2D graphics environment. Computing in Science & Engineering, 9(3), 90–95. DOI:10.1109/MCSE.2007.55

[15] Loke, M. H. (2014). Tutorial: 2D and 3D electrical imaging surveys. Geotomo Software Malaysia. https://www.geotomosoft.com

[16] Reynolds, J. M. (2011). *An introduction to applied and environmental geophysics* (2nd ed.). Wiley-Blackwell.

[17] Zohdy, A. A. R. (1989). A new method for the automatic interpretation of Schlumberger and Wenner sounding curves. *Geophysics*, 54(2), 245–253. DOI:10.1190/1.1442648

[18] Mavko, G., Mukerji, T., & Dvorkin, J. (2009). *The rock physics handbook: Tools for seismic analysis of porous media* (2nd ed.). Cambridge University Press.

[19] Telford, W. M., Geldart, L. P., & Sheriff, R. E. (1990). *Applied geophysics* (2nd ed.). Cambridge University Press.

[20] Rücker, C., Günther, T., & Wagner, F. M. (2017). pyGIMLi: An open-source library for modelling and inversion in geophysics. *Computers and Geosciences*, 109, 106–123. DOI:10.1016/j.cageo.2017.07.011

[21] Palmer, D. (1980). *The generalized reciprocal method of seismic refraction interpretation*. Society of Exploration Geophysicists.

[22] Virtanen, P., Gommers, R., Oliphant, T. E., Haberland, M., Reddy, T., Cournapeau, D., Burovski, E., Peterson, P., Weckesser, W., Bright, J., van der Walt, S. J., Brett, M., Wilson, J., Millman, K. J., Mayorov, N., Nelson, A. R. J., Jones, E., Kern, R., Larson, E., & SciPy 1.0 Contributors. (2020). SciPy 1.0: Fundamental algorithms for scientific computing in Python. *Nature Methods*, 17(3), 261–272. DOI:10.1038/s41592-019-0686-2 Python. *Nature Methods*, *17*(3), 261–272. https://doi.org/10.1038/s41592-019-0686-2